Coupling of the Reisomerization of the Retinal, Proton Uptake, and Reprotonation of Asp-96 in the N Photointermediate of Bacteriorhodopsin†

Andrei K. Dioumaev,‡,§ Leonid S. Brown,‡,§ Richard Needleman,|| and Janos K. Lanyi*,‡

Department of Physiology & Biophysics, University of California, Irvine, California 92697, and Department of Biochemistry, Wayne State University, Detroit, Michigan 48201

Received May 21, 2001; Revised Manuscript Received August 6, 2001

ABSTRACT: In the N to O reaction of the bacteriorhodopsin photocycle, Asp-96 is protonated from the cytoplasmic surface, and coupled to this, the retinal isomerizes from 13-cis,15-anti back to the initial all-trans configuration. To dissect the two steps, and to better understand how and why they occur, we describe the properties of two groups of site-specific mutants in which the N intermediate has greatly increased lifetime. In the first group, with the mutations near the retinal, an unusual N state is produced in which the retinal is 13-cis,15-anti but Asp-96 has a protonated carboxyl group. The apparent pK_a for the protonation is 7.5, as in the wild-type. It is likely that here the interference with N decay is the result of steric conflict of side-chains with the retinal or with the side-chain of Lys-216 connected to the retinal, which delays the reisomerization after protonation of Asp-96. In the second group, with the mutations located near Asp-96 or between Asp-96 and the cytoplasmic surface, reprotonation of Asp-96 is strongly perturbed. The reisomerization of the retinal occurs only after recovery from a long-living protein conformation in which reprotonation of Asp-96 is either entirely blocked or blocked at low pH.

The sequence of protonation and deprotonation reactions during the photoreaction cycle of bacteriorhodopsin, the light-driven proton pump of halobacteria (*1, 2*), consists of (i) deprotonation of the retinal Schiff base, (ii) protonation of Asp-85, a residue located on the extracellular side, and the coupled release of a proton to the extracellular surface, (iii) reprotonation of the Schiff base by Asp-96 located on the cytoplasmic side and reprotonation of Asp-96 from the cytoplasmic surface, and, finally, (iv) deprotonation of Asp-85 which restores the initial protonation state of the ionizable groups in the extracellular region. These steps of the transport cycle are the rationale for the "photocycle," described as the sequence of the interconversions of the spectroscopically defined J, K, L, M, N, and O chromophore and protein states. The recent crystallographic description (*3, 4*) of the structures of two photocycle intermediates in which the Schiff base is unprotonated ("early" and "late" M states) revealed that the events in the extracellular region are initiated by the changes at the Schiff base of the distorted photoisomerized retinal, while those in the cytoplasmic region are caused by gradual movement of the 13-methyl retinal group. Thus, relaxation of the photoisomerized retinal to a 13-cis,15-anti configuration free of conflict with the binding pocket is directly implicated in ensuring the directionality of the transport.

A high-resolution structure is not available for the N state, where the proton conduction pathway between Asp-96 and the Schiff base would be evident. It appears from the crystallographic structures of the various M states described (*3*−*5*) that, as generally assumed, the proton transfers to and from Asp-96 will rely on bound water molecules because they begin to form a hydrogen-bonded network in the M state already. Entry of water would be facilitated by the large-scale conformational change of the cytoplasmic segments of helices F and G, known from low-resolution difference maps of M and N in projection and in 3-dimensions (*6*−*10*), and distance changes and mobility changes of strategically placed spin-labels (*11, 12*). Two models have been proposed. The first model (*9, 13*) is based on projection maps for M and N. It considers the M and N states as having essentially the same protein conformation. This conformation is approximated by the structure of the unilluminated D96G/F171C/F219L triple mutant, determined by cryo-electron microscopy to 3.2−3.5 Å resolution (*13*). The conformational shift in these photointermediates creates a proton-transfer pathway between the Schiff base and the cytoplasmic surface. The pathway consists of a "channel," occluded in BR by numerous bulky hydrophobic side-chains, but opened by movement of helix F in M and N so that it admits water molecules. In this simple view, bacteriorhodopsin cycles through two principal protein conformations only, a BR-like state and an M-like state.

In the second model (*4*), the partial hydrogen-bonded network of water in M becomes long enough to connect Asp-96 with the protonated Schiff base during the decay of the M state, but it is replaced by another at the cytoplasmic surface so Asp-96 can be reprotonated from the bulk during the decay of N. Indeed, spin-labels at the cytoplasmic interhelical loops indicated that the structural changes in M and N are clearly distinguishable (*11, 12, 14, 15*), and a

† This work was supported partly by grants from the National Institutes of Health (to J.K.L., GM 29498) and the Department of Energy (to J.K.L. and R.N., DEFG03-86ER13525).

* To whom correspondence should be addressed. Telephone: (949) 824-7150. Fax: (949) 824-8540. E-mail: jlanyi@Orion.oac.uci.edu.

‡ University of California, Irvine.

§ Equal contributions.

|| Wayne State University.

10.1021/bi011027d CCC: $20.00
Published on Web 08/31/2001

recent time-resolved X-ray diffraction experiment detected three different structural components that should correspond to M, N, and BR (*16*).

A two-step conformational change would be consistent with the observation that introduction of bulky chemical labels on helix F and its cross-linking (*17*), as well as several single-residue mutations in the cytoplasmic region (*18*), have opposite consequences for M decay and N decay: the former is made more *rapid*, and the latter is made *slower*. A related finding is the negative cooperativity for the rate of M decay, but positive cooperativity for the decay of N (*19, 20*). These cooperativities will have originated from increase of lateral pressure in the plane of the membrane, the result of steric interference of bacteriorhodopsin molecules with one another in the purple membrane lattice. For this to occur, there would have to be large-scale conformational changes that *increase* the cross-section of the protein during M decay but *decrease* it during N decay. Thus, M and N could not have the same overall conformation. Distinct protein conformations in the reprotonation of the Schiff base and the reprotonation of Asp-96 are predicted on the grounds that the proton exchange between the Schiff base and Asp-96 is not dependent on $[H^+]$ in the pH range near the pK_a of Asp-96 (7−7.5) during the M to N equilibrium (*21*). Thus, at this time Asp-96 does not communicate with the bulk. Such communication is established when Asp-96 is reprotonated from the cytoplasmic surface, which in the wild-type protein occurs in the N to O reaction. The crystallographic structure of an O-like mutant of bacteriorhodopsin, to 2.2 Å resolution, in which the appearance of as many as nine additional water molecules between Asp-96 and the cytoplasmic surface was noted (*22*), confirms this model.

The change of helix F appears to consist of a rigid-body tilt, and in N, at least, an additional counterclockwise rotation as viewed from the cytoplasmic side (*12*). The tilt was detected in the 3-dimensional X-ray diffraction maps of the M state also, at 1.8 and 2.25 Å resolutions (*4, 5*), although with lower amplitudes. More specifically, comparison of the structures of the "early" and "late" M states (*3, 4*) indicated that the conformational shift in the cytoplasmic region is coupled to motions of the retinal by a chain of hydrogen bonds and covalent bonds that links Trp-182 at the 13-methyl retinal group and Thr-46 near the cytoplasmic surface, and by steric interactions of the side-chains of residues Thr-178, Leu-181, and Phe-219, located between helices F and G.

We are now in the position to begin to evaluate specific mutant phenotypes in terms of high-resolution structures. In this report, we describe the properties of the N states in two groups of mutants, one exemplified by V49A (near the retinal) and another by T46V (near Asp-96), to dissect the influences that govern the photocycle events during the N to O transition: the reisomerization of the retinal and its coupling to the protonation state of Asp-96, the possible modulation of the pK_a of Asp-96, and the establishment of a pathway for proton transfer between the cytoplasmic surface and Asp-96. The results indicate that, depending on their location and therefore their differing influences on these steps, the two kinds of mutations stabilize N states which differ in the way Asp-96 becomes reprotonated. Further, the structural requirements for the protonation of the Schiff base and the protonation of Asp-96 are separated and distinguished from one another.

MATERIALS AND METHODS

Purple membranes were prepared from *Halobacterium salinarum* by a standard method (*23*). The F42C, F42C/D96N, T46C, T46V, T46V/D96N, T46V/D115N, T46V/D96N/D115N, T46V/D36N/D38N/D102N/D104N, V49A, V49A/D96N, V49A/D115N, L93M, L100C, F171C, F171C/D96N, F219L, L223C, and S226C mutants were constructed as described before (*24*), and isolated after expression in *H. salinarum* as purple membrane patches.

Samples for the FTIR measurements were prepared by drying approximately 16 nmol of the protein on a CaF_2 window under mild vacuum. After drying, the films were soaked for 30−40 min in 50 mM MES, BTP, or succinate buffer at the specified pH. This procedure is as described previously (*25*). A 6 μm Teflon spacer (Harrick, Ossining, NY) was used to fix the sample thickness. All measurements were done at either 5 or 25 °C, using a temperature-controlled sample holder (Harrick) connected to a water bath (RTE-111, Neslab, Portsmouth, NH).

The FTIR measurements were performed under OPUS software on a model IFS-66s instrument (Bruker, Germany), at 2 cm^{-1} resolution. In the time-resolved mode, interferograms were collected in the "rapid-scan single side" mode (84 ms per scan). The IR detector was equipped with a 2000 cm^{-1} cutoff filter (Optical Coating Laboratory, Inc., Santa Rosa, CA). Excitation was provided by the second harmonics of the Nd:YAG laser (Surelite II or Minilite II, Continuum, Santa Clara, CA) at 532 nm, with ~7 ns pulse width, and ~2 mJ/cm^2 pulse energy. The laser pulses were spaced at times greater than 5× the slowest decay time-constant. A custom-built program provided the triggering of spectrometer, allowing one full scan before the arrival of the excitation flash from which the baseline was calculated. Kinetic analysis of data was with a program described before (*26*).

Static FTIR measurements were recorded on photostationary mixtures produced at 5 °C under illumination with a 175 W Cermax xenon lamp (ILC Technology, Sunnyvale, CA) through a high-pass cutoff visible filter (>580 nm), a glass heat filter, and a 5-mm-diameter, 2-m-long liquid waveguide. The light intensity at the sample was approximately 300 mW/cm^2. Difference spectra were obtained by subtracting the "background spectrum", measured with the light off, from the data-file measured under illumination ("signal"). Each "signal" measurement was preceded by 2 min of pre-illumination, while that of the "background" was preceded by 2 min of darkness, respectively. For each file (either "signal" or "background"), 558 scans were co-added, and the "light on/off" sequence was repeated 4 times. A water-vapor spectrum was subtracted until the baseline became flat in the 1800−1900 cm^{-1} region. The spectra obtained under these conditions were virtually indistinguishable from those obtained by kinetic analysis from time-resolved traces, and used only in Figures 9 and 10.

Kinetic measurements in the visible were done as described earlier, either on the same films prepared for FTIR, immediately before or after those measurements, or on membranes in suspension or encased in a polyacrylamide gel. For more details, and for measurements of proton kinetics with pyranine, see ref (*27*). Chemical modification of cysteines with methylmethane thiosulfonate (MMTS) was as described before (*17*).

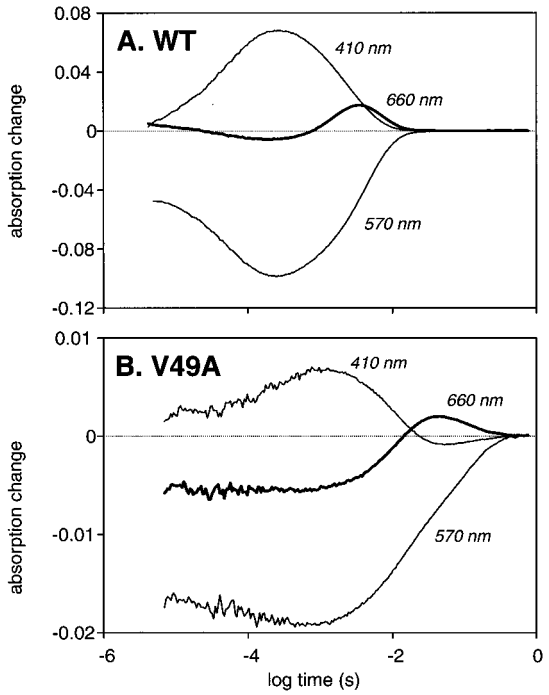

FIGURE 1: Chromophore kinetics in wild-type bacteriorhodopsin (A) and the V49A mutant (B). Absorption changes after pulse photoexcitation were followed at 410, 570, and 660 nm, and are shown on a logarithmic time-scale. As described earlier (*43*), the transient accumulation of M in the V49A photocycle is about 15% of the wild-type, which accounts for the smaller amplitude of the absorption changes. Conditions: 1 M NaCl, pH 5.9 (A), pH 6.1 (B), 25 °C.

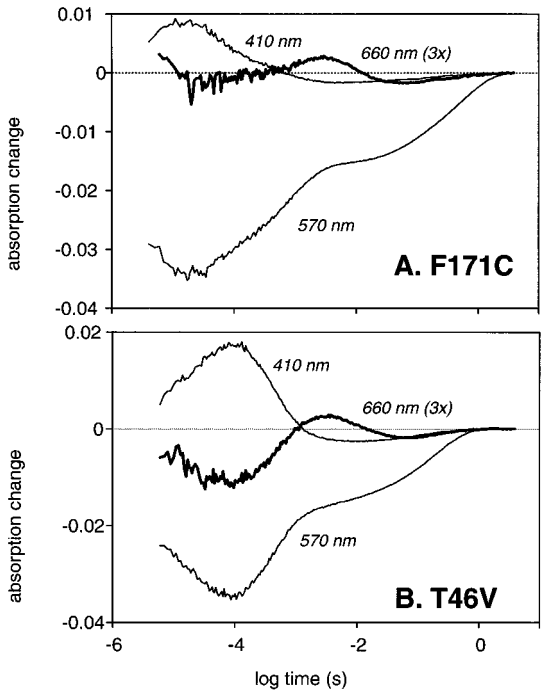

FIGURE 2: Chromophore kinetics in the F171C bacteriorhodopsin mutant (A) and in T46V (B). Absorption changes after pulse photoexcitation were followed at 410, 570, and 660 nm, and are shown on a logarithmic time-scale. Conditions: as in Figure 1, pH 5.6 (A), pH 6.3 (B).

RESULTS

Kinetic Description of the Photochemical Cycles of the V49A, F171C, and T46V Mutants. Figures 1 and 2 show transient absorption changes at 410, 570, and 660 nm after flash photoexcitation of the wild-type protein and three mutants in which the N state exhibits unusually slow decay. The changes at 410 nm describe proton transfer from and to the retinal Schiff base, i.e., the formation and decay of the M state, because extinction at this wavelength is greater when the Schiff base is unprotonated. The change at 570 nm originates from depletion of the BR state, but when M is absent, absorption at this wavelength detects also the N state, which has a somewhat blue-shifted maximum and lower extinction. The presence of the O state does not affect absorption here because O shows an isosbestic point near this wavelength (*28*). Instead, in the time-range studied, the strongly red-shifted O state could be followed at 660 nm (Figures 1 and 2, traces in boldface).

The results for the wild-type protein and V49A in Figure 1A,B show the sequence of absorption changes expected from the well-established "M-N-O" sequence and the equilibration of these states [as reviewed in (*29*)]. Thus, the M state (increased absorption at 410 nm) is followed by the N state (persistence of lowered absorption at 570 nm beyond the changes at 410 nm), and the O state (increased absorption at 660 nm). In both samples, the decay time-constants of N and O are the same (Figure 1A,B), suggesting decay of an equilibrium mixture of N and O to the initial BR state. This is not the case for F171C and T46V, however (Figure 2A,B). The N state persists well beyond the decay of the O state (N decay was slower than 100 ms vs 10 ms for O decay). Such unexpected kinetics, which at first sight imply an "M-O-N" reaction sequence, have been reported before (*30*). Additionally, the decay of the M state is considerably more rapid (by nearly an order of magnitude of time) than in the wild-type. For F171C, the amount of M accumulated is strongly depressed because of its unusually rapid decay (Figure 2A).

The two mutations T46V and V49A define, therefore, two classes with slow N decay, that either deviate or do not deviate from the wild-type pattern of M and O kinetics. We have identified some other members of these classes. The L93M mutant[1] belongs to the V49A class. The class with the anomalous "M-O-N" pattern and unusually rapid M decay includes F42C, T46C, L100C, L223C, and S226C, in addition to T46V and F171C. As discussed below, the locations of these groups of residues in the crystallographic structure suggest rationales for the different phenotypes detected.

Although it might be expected that the kinetics of the N and O states would depend critically on the reprotonation of Asp-96, the properties of D96N double mutants indicated that in the second class of mutants this was not so. With azide (10 mM at pH 5) included to accelerate the greatly slowed decay of the M state so the N and O intermediates would accumulate in observable amounts (*30*), the F42C/D96N, T46V/D96N, and F171C/D96N mutants exhibited N decay in the seconds time-range and the same anomalous "M-O-N" pattern as the F42C, T46V, and F171C single mutants (data not shown). Such kinetics, therefore, must

[1] Because it is red-shifted, in some reports (*31*−*33*) the last observable photointermediate of Leu-93 mutants is referred to as an "O" state. In molecular terms, however, one should consider it an N state because it contains a protonated Schiff base and 13-*cis*,15-*anti*-retinal.

Scheme 1

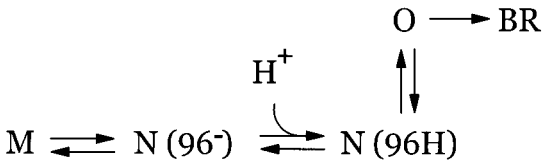

originate mostly from factors other than Asp-96 (e.g., not a changed pK_a). In fact, in the presence of azide, decay of O before decay of N was observed even in the single D96N mutant, where the lifetime of N is about 70 ms (*34*).

In the following, we attempt to interpret the differences in the rise and decay of the N and O states in terms of kinetic schemes. A great deal of earlier FTIR spectroscopy had indicated that there exists at least one N state, with 13-*cis*-retinal and unprotonated Asp-96 (*35*), and at least one O state, with *all-trans*-retinal and protonated Asp-96 (*36*). They have been placed sequentially in the photocycle before recovery of the BR state. Because the N to O reaction involves changes along two different reaction coordinates, i.e., reprotonation of Asp-96 and reisomerization of the retinal, it was postulated (*37*) that the two steps would be separable. The observation that in the D85N/F42C mutant deprotonation of Asp-96 at raised pH caused thermal isomerization to 13-cis,15-anti *in the dark* (*38*) suggested that the isomerization state of the retinal depends on the protonation state of Asp-96. If this principle applies to the photocycle as well (the evidence in favor of this is reviewed in ref *21*), the reprotonation of Asp-96, that removes the negative charge of the aspartate, drives the reisomerization to all-trans, and not the reverse. This idea is consistent with a report of two successive N states under some conditions, one with deprotonated Asp-96 followed by another with reprotonated Asp-96 (*39*), as we find here also. These N states can be most easily explained in terms of a proton-uptake-dependent conversion of N (96^-) to N (96H), where the ionization state of Asp-96 is indicated within the parentheses.

Scheme 1 explains the N and O kinetics in the group of mutants represented by V49A (Figure 1B), and probably in the wild-type, but not the N and O kinetics of the group represented by T46V (Figure 2A,B). In these mutants, the decay of N is considerably slower than the decay of O, and the O state does not accumulate in large amounts. While a kinetic scheme with two consecutive N states followed by O, and reversible reactions, allows both a low accumulation of O and a slow N decay as the last apparent step of the photocycle, it does require that the decays of N and O have the same time-constant. This is not observed. A second model (Scheme 2) with another N (96^-), different in conformation, termed N_{conf}, and in a cul-de-sac, explains the anomalous kinetics, assuming that the rate constant of the N (96^-) → N_{conf} transition is the fastest, and that of the N_{conf} → N (96^-) transition the slowest, of all the rates. We have not been able to find a simpler alternative to this scheme. An earlier model, branched at M (*40*), is far more complex.

This scheme creates an apparent very slow decay for N_{conf}, with a time-constant equal to or slower than the rate of the N_{conf} → N (96^-) transition. Thus, the observed rate of N decay can be slower (depending on the rate constants, much slower) than the O decay which will have the approximate

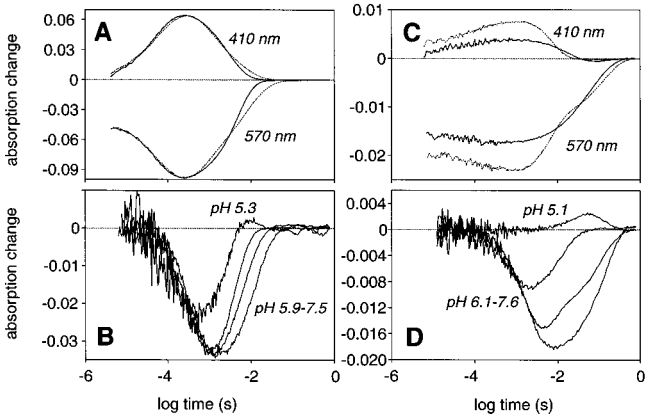

FIGURE 3: Chromophore and proton kinetics in wild-type bacteriorhodopsin (panels A and B, respectively) and the V49A mutant (panels C and D, respectively). Absorption changes after pulse photoexcitation were followed at 410 and 570 nm [panel A, pH 5.3 (solid line) and 7.5 (dotted line); and panel C, pH 5.1 (solid line) and 7.6 (dotted line)], and are shown on a logarithmic time-scale. Absorption increase of the pH indicator, pyranine, indicates proton uptake. They are shown for the wild-type (panel B, at pH 5.3, 5.9, 7.0, and 7.5, in order of increasing time-constants for uptake) and for V49A (panel D, at pH 5.1, 6.1, 7.1, and 7.6, in order of increasing time-constants for uptake). Conditions: 1 M NaCl, 25 °C.

Scheme 2

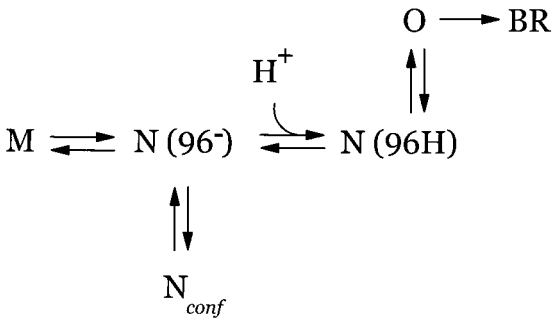

rate of the O → BR transition. Our simulations of this model (not shown) gave traces similar to those in Figure 2. Although the presence of N (96H) is not necessary in this kinetic scheme, Asp-96 has to reprotonate to recover the initial BR state, and we included it at its place in Scheme 1.

Proton Release and Uptake during the Photochemical Cycles of the V49A, F171C, and T46V Mutants. Proton release to the extracellular surface normally occurs during the rise of M, and proton uptake at the cytoplasmic surface during the N to O transition (*41*, *42*). Figures 3 and 4 show the time-courses of absorption changes of the pH indicator dye pyranine (panels B and D in each figure; absorption increase corresponds to pH rise, i.e., proton uptake) after photoexcitation at various pH values, together with absorption changes of the chromophore at 410 and 570 nm (panels A and C in each figure).

As well-known for the wild-type protein, the decay of the N state shows only minor changes in the pH 5−7 region (Figure 3A). This is consistent with minor slowing of proton uptake when the pH is raised from 6 to 7. A different kind of change is seen at lower pH because when the pH is set well below the pK_a for proton release (to the extracellular surface), proton release is delayed until the last step of the photocycle, and proton uptake (from the cytoplasmic surface)

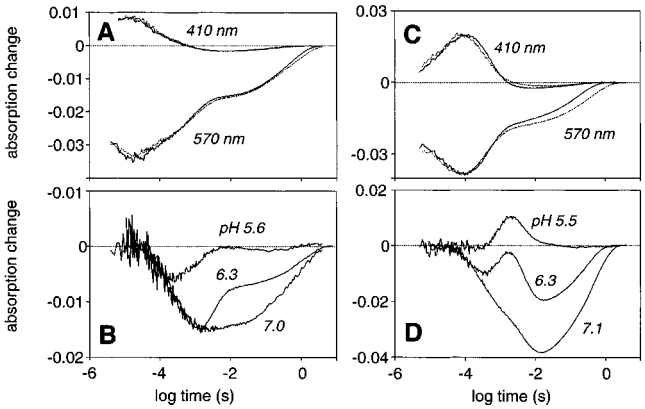

FIGURE 4: Chromophore and proton kinetics in the F171C bacteriorhodopsin mutant (panels A and B, respectively) and in T46V (panels C and D, respectively). Absorption changes after pulse photoexcitation were followed at 410 and 570 nm [panel A, pH 5.6 (solid line) and 7.0 (dotted line); and panel C, pH 5.5 (solid line) and 7.1 (dotted line)], and are shown on a logarithmic time-scale. Absorption increase of the pH indicator, pyranine, indicates proton uptake. They are shown for F171C (panel B, at pH 5.6, 6.3, and 7.0, in order of increasing time-constants for uptake) and for T46V (panel D, at pH 5.5, 6.3, and 7.1, in order of increasing time-constants for uptake). Conditions: 1 M NaCl, 25 °C.

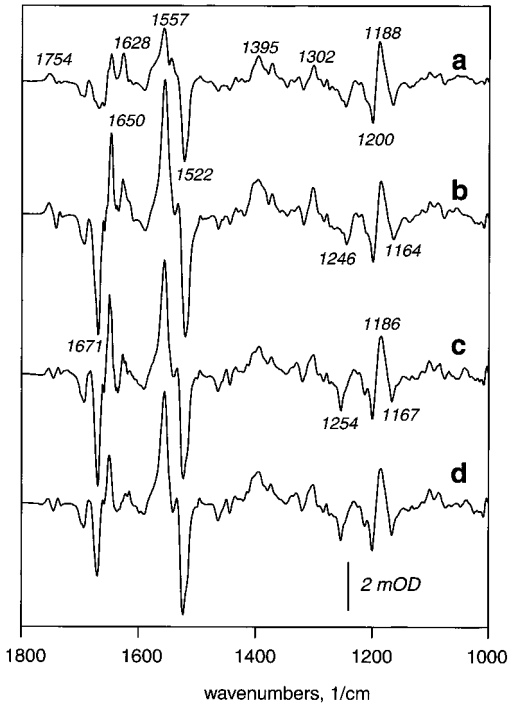

FIGURE 5: FTIR difference spectra after laser photoexcitation of the bacteriorhodopsin mutants V49A at pH 6.0 and 8.5 (a and b) and T46V at pH 6.1 and 8.0 (c and d). Spectra shown are the last kinetic components, which decay with time-constants of 1, 7, 3, and 30 s, for a, b, c, and d, respectively. The traces were normalized to the amplitude difference between 1200 and 1187 cm^{-1}.

occurs first (*42*). At intermediate pH, the high-pH and low-pH patterns of proton kinetics overlap, as at pH 5.3 in Figure 3B.

As in the wild-type, in V49A the time-constants of N are affected by pH only in a minor way, although the decay of N is slower than in the wild-type at any pH. The amount of the M state accumulated is strongly decreased at lower pH (Figure 3C), because the L to M equilibrium is shifted in favor of L (*43*). At pH 5.1, only net proton uptake is observed, suggesting that the pK_a for proton release is higher than in the wild-type (compare Figure 3D with Figure 3B). More important for this study, however, proton uptake between pH 6 and 8 shows kinetics greatly changed from the wild-type (Figure 3D). At pH 6, proton uptake correlates with the decay of M (τ = 11 ms); i.e., it is more rapid (by an order of magnitude of time) than the decay of N (τ = 100 ms), but at pH near 8, it is concurrent with N decay. At intermediate pH, both phases of proton uptake are seen, and as the pH is increased, the slow component replaces the rapid one. The time-constants of the two kinetic components are much less affected by pH than their relative amplitudes.

Such proton uptake kinetics were reported earlier for T46V/R227Q (*18*), and W182F (*39*), although in less detail. The mutants of the other kinetic class described above, exemplified in Figure 4 by F171C and T46V, also show the biphasic proton uptake. The decay of absorption change in F171C becomes slightly slower with increasing pH at both 410 and 570 nm (Figure 4A), but more dramatic is the fact that proton uptake is rapid at pH 5.6 (approximately 2 ms) and slow (hundreds of milliseconds) near pH 7, concurrent with the much slower decay of N. At a pH between these values, the proton kinetics are biphasic (Figure 4B). The pattern of proton kinetics in T46V is complicated by the fact that the signals from proton release and uptake overlap in time. This is because the pK_a for proton release in this mutant is elevated even more than in the V49A and F171C mutants, and therefore the rapid uptake causes net alkalinization at pH as high as 5.5 (Figure 4D). Nevertheless, it is evident that there is rapid proton uptake at lower pH, and increasingly dominant slow uptake at higher pH, in this mutant also. Proton uptake much more rapid than the decay of N was reported before for the T46V/R227Q mutant (*18*). The apparent pK_a for rapid proton uptake is estimated to be about 6 in both T46V and F171C.

All other mutants that exhibit slow N decay and the anomalous apparent "M-O-N" pattern, i.e., F42C, L100C, L223C, and S226C (data not shown), take up protons in the biphasic pH-dependent manner illustrated for F171C and T46V in Figure 4.

Protonation State of Asp-96 in the N States of the V49A and T46V Mutants. Figure 5 shows difference FTIR spectra for V49A at pH below and above the pK_a for proton uptake, and for T46V, at similar pH values (spectra for the other mutants are not shown, but were similar). The spectra are the result of global fitting of the data between the instrumental time-resolution (approximately 100 ms) and the end of the photocycle, and represent the last, main kinetic component present. The frequencies and relative amplitudes of the C−C stretch bands at 1164−1167, 1186−1188, and 1200 cm^{-1} identify the N intermediate unambiguously, as do the coupled N−H and C−H bend modes at 1302 and 1395 cm^{-1} (*35*, *36*). The pair of positive and negative amide bands are also at the frequencies and with the amplitudes expected for N, except for the low-pH trace of the V49A mutant (Figure 5a) where they have less amplitude. The somewhat lower amplitude of the Asp-85 C=O stretch band indicates that, as found before for this mutant (*43*), at low pH the L state persists until the end of the photocycle. The presence of L, together with N, accounts partially for the smaller amide bands because in L they are not prominent. Additionally, the negative amide band, in particular, may

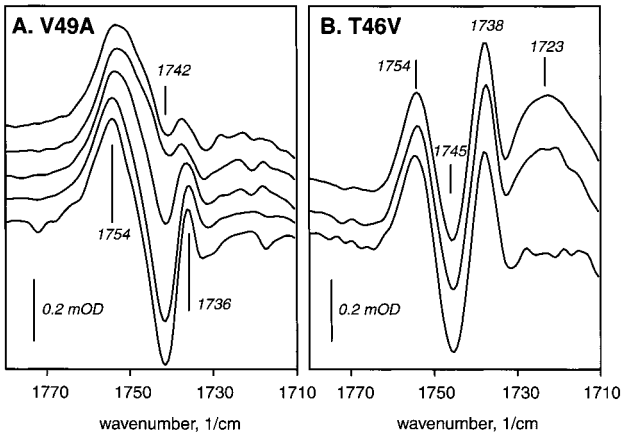

FIGURE 6: FTIR difference spectra for the V49A (A) and T46V (B) bacteriorhodopsin mutants in the C═O stretch region, as in Figure 5. In (A), the pH was 5.0, 6.1, 7.6, 8.2, and 8.8 (from top to bottom). In (B), the pH was 5.0, 6.2, and 7.7 (from top to bottom). Spectra were measured as in Figure 5, but at various pH values.

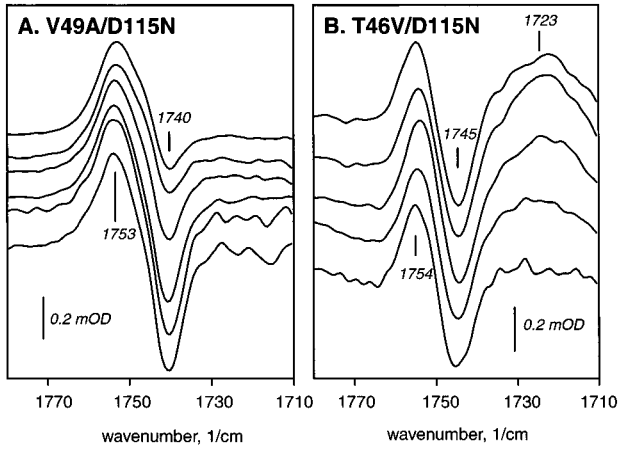

FIGURE 7: FTIR difference spectra for the V49A/D115N (A) and T46V/D115N (B) bacteriorhodopsin mutants in the C═O stretch region, as in Figure 5. In (A), the pH was 5.0, 6.1, 7.5, 8.2, 9.0, and 9.5 (from top to bottom). In (B), the pH was 4.0, 5.0, 6.2, 7.0, and 8.0 (from top to bottom). Spectra were measured as in Figure 5, but at various pH values.

be pH dependent in the N state of V49A. The FTIR spectra for both V49A (Figure 5a,b) and T46V (Figure 5c,d) indicate that there is little contribution from the M or O intermediates, if any; i.e., the retinal is 13-cis and the Schiff base is protonated, as it should be in N. Uniquely in V49A, the 1254 cm^{-1} band, ascribed to $C_{12}-C_{13}$ stretch in the retinal and Lys-216 side-chain rocking motion (*44*), is shifted to 1246 cm^{-1}.

In Figure 6 the 1800−1710 cm^{-1} region is enlarged to show the C═O stretch bands of the protonated COOH groups in V49A and T46V at different pH values. The amplitude of the negative band from Asp-96 at 1742 cm^{-1} in V49A is less when the pH is lower and nearly disappears at pH 5 (Figure 6A). Thus, at low pH Asp-96 becomes reprotonated well before the decay of N. This is consistent with the observation of rapid proton uptake at lower pH (Figure 4C), and the idea of a second N state of this mutant, with the retinal still 13-cis,15-anti, but Asp-96 unprotonated at high pH and protonated at low pH.

Remarkably, however, although at pH 5−6 there is proton uptake in T46V also (Figure 4D), the negative band of Asp-96, here at 1745 cm^{-1}, persists. In fact, the band appears to be nearly pH independent in magnitude (Figure 6B). On the other hand, a broad positive band centered at about 1723 cm^{-1}, not observed in the N state of the wild-type protein (not shown) or in the V49A mutant (Figure 6A), is seen. The band is present in the N state of F42C also (not shown). Bands in this frequency region originate, without any ambiguity, from protonated carboxyls. There are two possible explanations for the 1723 cm^{-1} band. The first alternative is that it is the shifted band of reprotonated Asp-96. Indeed, in the spectrum of N in the T46V/D96N double mutant, produced in the presence of azide to accelerate the rate of M decay, the band was absent (not shown). The second alternative is that Asp-96 is unprotonated and the positive 1723 cm^{-1} band arises from protonation of another carboxylate group that was initially unprotonated.

The band from Asp-96 in the spectra in Figure 6 is partly overlapped by spectral features of Asp-115, whose band is known to shift from 1734 to 1738 cm^{-1} in the N state of the wild-type (*45*), and a similar shift occurs in the V49A mutant also. Possibly because of the shifted negative band of Asp-96, the positive band for Asp-115 is particularly large in T46V, as well as in F42C and L223C (although not in L100C, F171C, and S226C; not shown). To remove this interference and thereby confirm the conclusions about the protonation state of Asp-96, the V49A/D115N and T46V/D115N mutants were examined (Figure 7). Comparison of these spectra with those of V49A and T46V is made possible by the fact that the proton kinetics were not changed by the D115N mutation (not shown). Unless a new band not normally seen is present, the region below 1735 cm^{-1} is now expected to be featureless, and this is indeed the case for V49A/D115N (Figure 7A). The negative Asp-96 band is shifted to its true, undistorted value of 1740 cm^{-1}. The pH dependence of the amplitude of this band is essentially the same as in V49A, as indicated in Figure 8 where this amplitude is shown for both V49A and V49A/D115N as a function of pH. The apparent pK_a is approximately 7.5. This should correspond to the pK_a of Asp-96 during its reprotonation in the N state. Estimated only approximately because of uncertainty over the extent the low-pH and high-pH proton kinetic patterns overlap (Figure 3D), the pK_a for proton

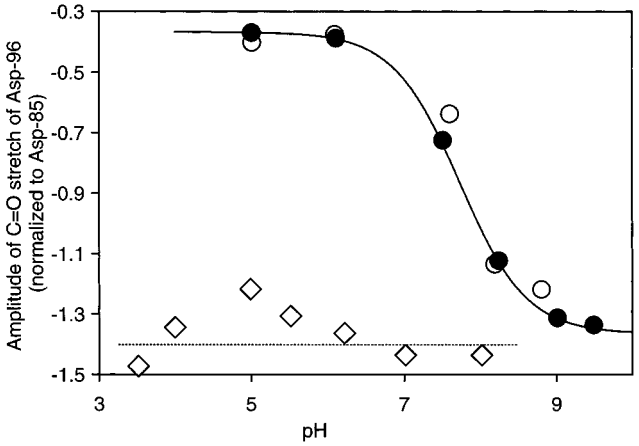

FIGURE 8: Amplitude of the negative C═O stretch band of the protonated Asp-96 in the N state, as a function of pH. V49A, open circles; V49A/D115N, closed circles; T46V/D115N, open diamonds. The amplitudes were normalized to the relatively pH-independent positive C═O stretch band of the protonated Asp-85.

uptake is about 7. The results with V49A indicate, therefore, that at pH < 7 proton uptake occurs well before the decay of N (Figure 3C,D), and Asp-96 becomes protonated (Figures 6A, 7A, and 8). This results in an unusual N state, in which the retinal is still 13-cis,15-anti, but Asp-96 is already reprotonated. At pH > 7, the more conventional N state is produced in which Asp-96 remains unprotonated until reisomerization of the retinal.

In T46V/D115N (Figure 7B), the negative band of Asp-96 is at 1745 cm^{-1}, i.e., 4−5 cm^{-1} higher than in the wild-type, as seemed to be the case in T46V (Figure 6B). From the second derivative of the absolute infrared spectra of unilluminated T46V and T46V/D115N (not shown), we obtained also such an unusually high frequency. The shift is to be expected from the fact that in the BR state of the T46V mutants the hydrogen bond between the COOH of Asp-96 and the side-chain of Thr-46 (*46*) will be missing. It was observed already in the L state of T46V (*47*). Additionally, Figure 7B confirms that the amplitude of the negative C═O stretch band of Asp-96 is unchanged between pH 4 and 8. The latter is evident also from Figure 8, where the amplitude is shown as a function of pH.

In the T46V/D115N mutant, the positive band at 1723 cm^{-1} can be discerned without any interference from other bands (Figure 7B). Its broadness suggests that it might originate from protonation of one or more carboxylates in a somewhat heterogeneous environment. The magnitude of the band, i.e., the extent of the protonation, is plotted vs pH in Figure 9A, with the results from T46V included as well. The band is maximal at pH ∼ 5, and decreases at both higher and lower pH, with half-maximal amplitudes at pH 3.8 and 6.3. The equation that describes this kind of behavior is the difference of two Henderson−Hasselbalch terms:

$$y = \frac{1}{1 + 10^{(\mathrm{pH}-\mathrm{p}K_a')}} - \frac{1}{1 + 10^{(\mathrm{pH}-\mathrm{p}K_a)}} \qquad (1)$$

where y is the protonation state at the pH in question and pK_a and pK_a' refer to the acid dissociation constants either of two different groups or of the same group but in the BR state and in the N state. Figure 9A contains calculated curves for the best fit, with pK_a and pK_a' values of 3.8 and 6.3, and an estimated uncertainty of ±0.4.

This bell-shaped pH dependence is unlike that of the Asp-96 depletion band at 1745 cm^{-1}, which is pH independent in this region (Figure 8). If the 1723 cm^{-1} band is assigned to protonated Asp-96, this aspartate must be unprotonated at both low and high pH. Thus, in this case, pK_a' refers to the protonation of Asp-96, but pK_a belongs to an unidentified group whose protonation *prevents* protonation of Asp-96. The two pK_as are interpreted differently if the 1723 cm^{-1} band belongs to the unidentified carboxyl group of the alternative model. In this case, the proton affinity of that group will have increased in the N state, resulting in its protonation at pH values between the initial pK_a and the transient pK_a', but not at lower pH where it is always protonated and at higher pH where it remains unprotonated. Absent in T46V/D96N, the shift of proton affinity would depend on the negative charge of the unprotonated Asp-96. The unidentified group thus behaves analogously to an indicator dye covalently attached to the surface of bacteriorhodopsin (*48*). It is difficult to decide between the two alternatives, because both predict interaction of Asp-96 with an unidentified group.

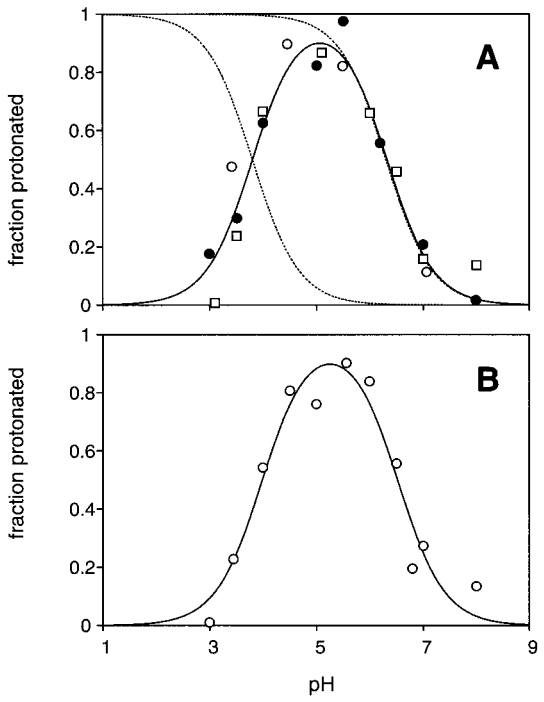

FIGURE 9: Magnitude of the broad positive feature at 1723 cm^{-1}, interpreted as the C═O stretch band of one or more COOH group(s) that become(s) protonated in the N state, as a function of pH. (A) Titration of the T46V and T46V/D115N mutants (squares and circles). (B) Titration of the T46V/D36N/D38N/D102N/D104N mutant. Open symbols, spectra from photostationary states; closed symbols, spectra from time-resolved experiments. The difference spectra between 1710 and 1795 cm^{-1} were fitted with a sum of Gaussians, and the areas under the band were normalized to the area of the band of Asp-85 at 1754 cm^{-1}. Similar results were obtained when the 1188 and 1200 cm^{-1} bands were used for the normalization. The values were then scaled to values between 0 and 1, corresponding to fractional protonation in eq 1. The two dashed lines in (A) refer to the calculated pK_as of the two components, 3.8 and 6.3, respectively, with uncertainties of ±0.4. The best fit of the data in (B) gave pK_as of 4.0 and 6.5. The solid lines are for the net protonation in the N state, calculated from the two sets of pK_as.

The candidates for the unidentified group are the aspartate and/or glutamate residues at the cytoplasmic surface (i.e., Asp-36, Asp-38, Asp-102, Asp-104, Glu-161, and Glu-166 on interhelical loops, and Glu-232, Glu-234, Glu-237, and Asp-242 on the C-terminal tail). Of these, Asp-36, Asp-38, Asp-102, and Asp-104 would be the most attractive possibilities for transiently protonated residues, because they are located on the cytoplasmic surface and several of them have been suggested to form a cluster that captures the proton that reprotonates Asp-96 (*49*, *50*). We measured the FTIR spectra of the multiple mutant T46V/D36N/D38N/D102N/D104N. In the C═O stretch region, the pH dependence of the broad band at 1723 cm^{-1} was similar to the T46V mutants without the four aspartic acid residues replaced (Figure 9B). Direct comparison of the FTIR spectra in the relevant region for T46V and T46V/D36N/D38N/D102N/D104N (Figure 10) illustrates the near-equivalence of the protonation band with and without the four aspartic acid residues in the protein. Further, the protonation pattern of pyranine during the photocycle of the T46V/D36N/D38N/D102N/D104N mutant was not significantly different from

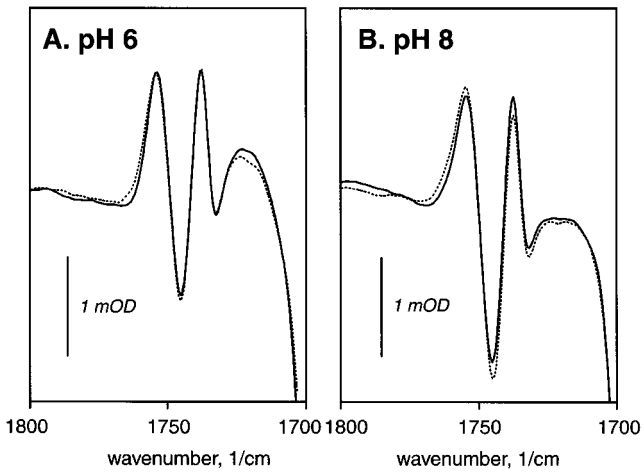

FIGURE 10: Difference spectra of the C=O stretch region for the T46V (solid traces) and the T46V/D36N/D38N/D102N/D104N (dashed traces) mutants, at pH 6 (A) and pH 8 (B).

that in T46V (not shown). This is consistent with our earlier report that the D36N, D38N, D102N, and D104N mutations have only small effects on the kinetics of N (*51*). If we exclude the four most obvious aspartic acid residues (*49, 50, 52, 53*), that leaves Glu-161, and Glu-166, on the E−F interhelical loop, and Glu-232, Glu-234, Glu-237, and Asp-242, on the C-terminal tail on the cytoplasmic side, and, less likely, Glu-9, Glu-74, Glu-194, or Glu-204, on the extracellular side, as candidates.

From these results, we can reconstruct the protonation events in the N state of T46V (and F42C) in accordance with the two alternative assignments of the 1723 cm^{-1} band. Both models implicate the mutated residues immediately adjacent to Asp-96 in the reprotonation of this aspartic acid, but lead to unanswered questions. In the first model, Asp-96 reprotonates well before reisomerization of the retinal with a pK_a of 6.3, i.e., about 1 pH unit lower than in the wild-type (*54*−*57*), and its C=O stretch in N_{conf} is shifted to lower frequency by about 20 cm^{-1}. Both shifts suggest perturbation of the environment of Asp-96, perhaps with increased hydration and more possibilities of hydrogen-bonding. However, in this model, protonation of an unidentified group, with a pK_a of 3.8, will block rapid reprotonation of Asp-96. In the second model, Asp-96 is not protonated even at pH as low as 4 during the lifetime of N_{conf}, and one or more unidentified carboxylates become protonated instead. At pH near 5, proton uptake results in the protonation of the carboxyl group(s). At pH well below 5 (pK_a = 3.8), they are protonated already in the BR state. Presumably, at such low pH there is no acceptor for the proton uptake, but this could not be determined with pyranine because its pK_a is 7.3. At pH well above 5 (pK_a' = 6.3), the carboxyl group(s) remain(s) unprotonated throughout the photocycle, and proton uptake is delayed until the decay of N (and recovery of the BR state). The proton uptake during M decay in this case leads to protonation of not Asp-96, as in V49A, but of the postulated unidentified carboxyl group(s).

Although the 1723 cm^{-1} band was expected in L100C, F171C, L223C, and S226C mutants, because at pH < 6 they show proton uptake concurrent with decay of M but no decrease in the negative C=O stretch band of Asp-96 during the lifetime of N (as do F42C and T46V), the FTIR spectra did not contain any features at 1720 cm^{-1} (not shown). The spectra of these mutants lack a positive band, and therefore there is no doubt that here the protonation of Asp-96 is blocked. The observed proton uptake depends on the cysteine residues introduced, because in F171C and S226C at least (where this could be tested without making the decay of N rapid), modification of the SH group with MMTS eliminated proton uptake before decay of N. The possibility exists, therefore, that the cysteine residues are transiently protonated in these mutants. However, we have not been able to detect such protonation in the S−H stretch region either at 2500−2600 cm^{-1} in H_2O or in the 1800−2000 cm^{-1} region in D_2O (*58*).

DISCUSSION

We have studied the N photointermediates of a variety of bacteriorhodopsin mutants, with the goal of dissecting the factors that affect the photocycle reactions immediately following the reprotonation of the retinal Schiff base: a change of the pK_a of Asp-96, the possibility of establishing a proton-transfer chain between the cytoplasmic surface and Asp-96, and the means of coupling the reisomerization of the retinal to all-trans to the protonation state of Asp-96. In all mutants examined, the decay of the N state is greatly slowed. Specifically, we tested the hypothesis that the region between Asp-96 and the cytoplasmic surface is capable of conformational changes that open or close a proton-transfer pathway separate from, or even contrary to, those that facilitate the reprotonation of the Schiff base (*21*). Thus, Asp-96 would be inaccessible to the bulk during the time it enters into a protonation equilibrium with the Schiff base, but become connected to the surface in the next photocycle step, the N ↔ O reaction. The results extend earlier findings (*18*) that some single-residue replacements near the cytoplasmic surface cause both strong *inhibition* of the protonation of Asp-96 and *acceleration* of the protonation of the Schiff base (Figure 2). These and the other results we report here support the hypothesis of sequential conformation changes.

The chromophore and proton kinetics in the two classes of mutants tested correlate with their locations in the protein. Figure 11 shows the structure of the cytoplasmic region of the M state, from X-ray diffraction data of the E204Q mutant at 1.8 Å resolution (*4*). The residues which influence the lifetime of the N state are color-coded according to their location and the phenotypes of their mutants, as described below.

Mutation of residues that contact the retinal or the side-chain of the connected Lys-216 (shown in green, Figure 11), such as Leu-93 (*33*) and Val-49 (*45*), might be expected to prolong the lifetime of the N state because they slow the reisomerization of the retinal. We find that in these mutants the reprotonation of Asp-96 is normal, but the reisomerization of the retinal is not necessarily concurrent with it, as under most conditions in the wild-type photocycle. Presumably, because of local steric conflicts, the retinal lags in its response to the reprotonation of Asp-96. The changed frequency of the combined C_{12}−C_{13} stretch and Lys-216 rock (spectra a and b in Figure 5) is consistent with the idea of changed steric constraint at the retinal. The kinetics indicate that the N states accumulate in the way they have been assumed for the wild-type; i.e., first an N with unprotonated Asp-96 is formed [N (96^-)], and at pH < 7 this is followed by

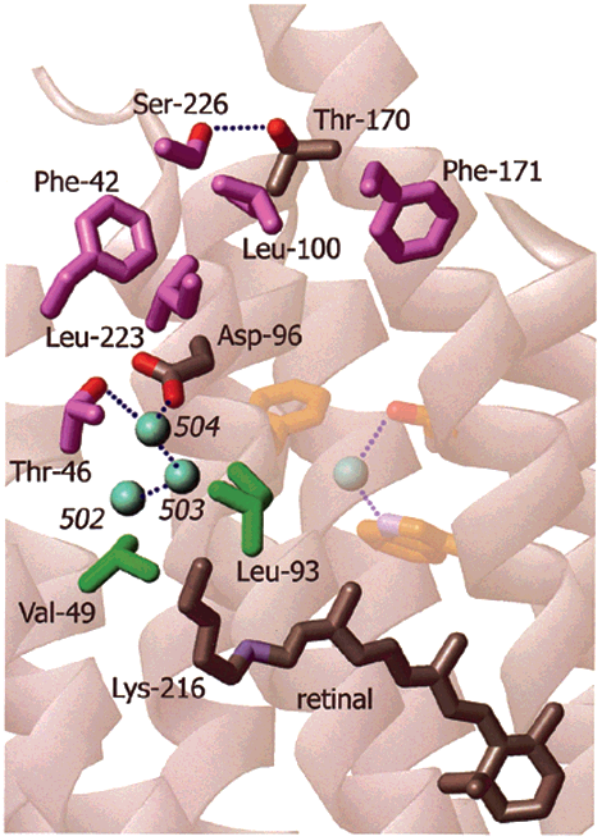

FIGURE 11: Structural model of the cytoplasmic region of the M state, from X-ray crystallography of the E204Q mutant (*4*). Residues whose mutation causes slow decay of the N intermediate, as discussed in the text, are shown in color. The color code is according to the suggested reasons for the long lifetime of N in the mutants: residues which through steric effect influence reisomerization of the retinal are green, and residues which affect the reprotonation of Asp-96 from the cytoplasmic surface are purple. Water molecules are in cyan; hydrogen-bonds are in blue. Some other residues that play a role in cytoplasmic events, as discussed in the introduction, and the transmembrane helices, are shown with decreased opacity.

reprotonation of Asp-96 from the cytoplasmic bulk, resulting in a second N, we termed N (96H). Thus, we observe the accumulation of either N (96^-) (at high pH) or N (96H) (at low pH), with an apparent pK_a of 7.5, i.e., roughly the same as earlier estimates of the pK_a of Asp-96 in the wild-type (*54*−*57*).

Mutations of residues at Asp-96 and between Asp-96 and the cytoplasmic surface, i.e., Thr-46, Phe-42, Leu-100, Phe-171, Leu-223, and Ser-226 (shown in purple, Figure 11), were expected to affect the reprotonation of Asp-96, by changing either its pK_a or its accessibility to the cytoplasmic surface, or both. An effect on the reisomerization of the retinal would be indirect, through the coupling mechanism to the protonation event. The involvement of Thr-46 in the protonation of Asp-96 is obvious, in view of the fact that it is hydrogen-bonded to it, directly in the BR state (*3, 46*) and via water 504 in the M state [Figure 11, (*4*)]. Phe-42, Leu-100, and Leu-223 should affect the pK_a of Asp-96 directly also, as they contribute to its hydrophobic environment. Indeed, we reported earlier from infrared titration of the D85N/F42C and D85N mutants (*38*) that the pK_a for Asp-96 in the double mutant was lowered by 1.5 pH units relative to D85N. The case for Phe-171 and Ser-226 is not so obvious, as these residues are further away from Asp-96 (Figure 11). The clue to their effect on Asp-96 is provided by Ser-226, which stabilizes a "closed" cytoplasmic conformation through its hydrogen-bonding to Thr-170, in which helices F and G are in closer proximity in BR and M than expected in the N state (Figure 11). Presumably, the more remote hydrophobic side-chains, like Phe-171 and perhaps also Leu-100, perform the same role by contributing to the shield over the cytoplasmic surface that excludes water, and by involvement in hydrophobic interaction with residues of the neighboring helix.

The common phenotype of the residues shown in Figure 11 in purple includes the trapping of the protein in a conformation with unusually long lifetime, and an apparently lowered pK_a for Asp-96 during its deprotonation (and perhaps also during its reprotonation). What happens to Asp-96 in this long-living state, termed N_{conf}, is subject to two different interpretations of the data (as discussed under Results). Asp-96 may be protonated with a shifted C═O stretch frequency, and its protonation is blocked when an unknown group with lower pK_a becomes protonated. This is possible in T46V and F42C, but not in the Leu-100, Phe-171, Leu-223, and Ser-226 mutants. In the latter mutants, Asp-96 remains unprotonated. Alternatively, in N_{conf} the protonation of Asp-96 is blocked in a wider pH range, allowing the transient protonation of other, unknown carboxyl group(s) instead. In either case, the mutations in purple perturb the region of Asp-96, i.e., a location ≥10 Å distant from the retinal. Because of this perturbation, or in some cases directly because the protonation of Asp-96 is blocked, reisomerization of the retinal is greatly slowed.

From the structure (Figure 11), it is evident that there is a hydrophobic shield between Asp-96 and the cytoplasmic surface. During the reprotonation of Asp-96, a proton-transfer pathway would have to be established in this region. Indeed, it has been suggested recently (*13*) that the side-chains of Phe-42, Leu-100, Thr-170, Phe-171, and Leu-223, i.e., the same residues (but one) we tested here, block proton entry into the cytoplasmic region, and the tilt of helix F creates an opening that increases proton access from the bulk. However, one would expect that if the side-chains were made smaller the opening should be wider rather than narrower. It is a paradox, therefore, that replacing the bulky side-chains that occlude the pore with smaller ones *blocks* reprotonation of Asp-96 (in L100C, F171C, L223C, and perhaps also in F42C). The fact that these mutations increase the rate of the reprotonation of the Schiff base, even as they decrease the rate of the reprotonation of Asp-96, indicates that the two proton transfers obey separate and opposite rules and therefore do not utilize a single channel. We suggest that proton transfer from the surface to Asp-96 is not via a pore but via a specific pathway that requires the interlocking of specific hydrophobic side-chains, and the pathway is absent in M and created in N to allow the rise of the O state. Interestingly, in the crystallographic structure of the O-like state (*22*), numerous new bound water molecules appear in the region of the hydrophobic shield. They appear to be fragmented parts of a network, hydrogen-bonded mostly to main-chain C═O groups in clusters of various sizes containing up to five connected water molecules. Presumably, they represent the remains of a more interconnected network that formed during the N to O reaction.

REFERENCES

1. Oesterhelt, D. (1998) *Curr. Opin. Struct. Biol. 8*, 489−500.
2. Lanyi, J. K. (1999) *FEBS Lett. 464*, 103−107.
3. Luecke, H., Schobert, B., Richter, H. T., Cartailler, J. P., and Lanyi, J. K. (1999) *Science 286*, 255−261.
4. Luecke, H., Schobert, B., Richter, H. T., Cartailler, J.-P., Rosengarth, A., Needleman, R., and Lanyi, J. K. (2000) *J. Mol. Biol. 300*, 1237−1255.
5. Sass, H. J., Büldt, G., Gessenich, R., Hehn, D., Neff, D., Schlesinger, R., Berendzen, J., and Ormos, P. (2000) *Nature 406*, 649−653.
6. Subramaniam, S., Gerstein, M., Oesterhelt, D., and Henderson, R. (1993) *EMBO J. 12*, 1−8.
7. Kamikubo, H., Kataoka, M., Váró, G., Oka, T., Tokunaga, F., Needleman, R., and Lanyi, J. K. (1996) *Proc. Natl. Acad. Sci. U.S.A. 93*, 1386−1390.
8. Sass, H. J., Schachowa, I. W., Rapp, G., Koch, M. H., Oesterhelt, D., Dencher, N. A., and Büldt, G. (1997) *EMBO J. 16*, 1484−1491.
9. Subramaniam, S., Lindahl, M., Bullough, P., Faruqi, A. R., Tittor, J., Oesterhelt, D., Brown, L., Lanyi, J., and Henderson, R. (1999) *J. Mol. Biol. 287*, 145−161.
10. Vonck, J. (2000) *EMBO J. 19*, 2152−2160.
11. Thorgeirsson, T. E., Xiao, W., Brown, L. S., Needleman, R., Lanyi, J. K., and Shin, Y. K. (1997) *J. Mol. Biol. 273*, 951−957.
12. Xiao, W., Brown, L. S., Needleman, R., Lanyi, J. K., and Shin, Y. K. (2000) *J. Mol. Biol. 304*, 715−721.
13. Subramaniam, S., and Henderson, R. (2000) *Nature 406*, 653−657.
14. Steinhoff, H. J., Mollaaghababa, R., Altenbach, C., Hideg, K., Krebs, M., Khorana, H. G., and Hubbell, W. L. (1994) *Science 266*, 105−107.
15. Rink, T., Pfeiffer, M., Oesterhelt, D., Gerwert, K., and Steinhoff, H. J. (2000) *Biophys. J. 78*, 1519−1530.
16. Oka, T., Yagi, N., Fujisawa, T., Kamikubo, H., Tokunaga, F., and Kataoka, M. (2000) *Proc. Natl. Acad. Sci. U.S.A. 97*, 14278−14282.
17. Brown, L. S., Váró, G., Needleman, R., and Lanyi, J. K. (1995) *Biophys. J. 69*, 2103−2111.
18. Brown, L. S., Yamazaki, Y., Maeda, A., Sun, L., Needleman, R., and Lanyi, J. K. (1994) *J. Mol. Biol. 239*, 401−414.
19. Tokaji, Z. (1995) *FEBS Lett. 357*, 156−160.
20. Váró, G., Needleman, R., and Lanyi, J. K. (1996) *Biophys. J. 70*, 461−467.
21. Balashov, S. P. (2000) *Biochim. Biophys. Acta 1460*, 75−94.
22. Rouhani, S., Cartailler, J.-P., Facciotti, M., Walian, P., Needleman, R., Lanyi, J., Glaeser, R. M., and Luecke, H. (2001) *J. Mol. Biol*. (in press).
23. Oesterhelt, D., and Stoeckenius, W. (1974) *Methods Enzymol. 31*, 667−678.
24. Needleman, R., Chang, M., Ni, B., Váró, G., Fornes, J., White, S. H., and Lanyi, J. K. (1991) *J. Biol. Chem. 266*, 11478−11484.
25. Dioumaev, A. K., Richter, H. T., Brown, L. S., Tanio, M., Tuzi, S., Saitō, H., Kimura, Y., Needleman, R., and Lanyi, J. K. (1998) *Biochemistry 37*, 2496−2506.
26. Dioumaev, A. K. (1997) *Biophys. Chem. 76*, 1−26.
27. Brown, L. S., Sasaki, J., Kandori, H., Maeda, A., Needleman, R., and Lanyi, J. K. (1995) *J. Biol. Chem. 270*, 27122−27126.
28. Ludmann, K., Gergely, C., and Váró, G. (1998) *Biophys. J. 75*, 3110−3119.
29. Lanyi, J. K., and Váró, G. (1995) *Isr. J. Chem. 35*, 365−385.
30. Drachev, L. A., Kaulen, A. D., and Komrakov, A. Y. (1992) *FEBS Lett. 313*, 248−250.
31. Delaney, J. K., Schweiger, U., and Subramaniam, S. (1995) *Proc. Natl. Acad. Sci. U.S.A. 92*, 11120−11124.
32. Delaney, J. K., and Subramaniam, S. (1996) *Biophys. J. 70*, 2366−2372.
33. Delaney, J. K., Subramaniam, S., Schmidt, P., and Atkinson, G. H. (1997) *J. Phys. Chem. B 101*, 5619−5621.
34. Brown, L. S., and Lanyi, J. K. (1996) *Proc. Natl. Acad. Sci. U.S.A. 93*, 1731−1734.
35. Pfefferle, J. M., Maeda, A., Sasaki, J., and Yoshizawa, T. (1991) *Biochemistry 30*, 6548−6556.
36. Hessling, B., Souvignier, G., and Gerwert, K. (1993) *Biophys. J. 65*, 1929−1941.
37. Fodor, S. P. A., Ames, J. B., Gebhard, R., Van den Berg, E. M. M., Stoeckenius, W., Lugtenburg, J., and Mathies, R. A. (1988) *Biochemistry 27*, 7097−7101.
38. Dioumaev, A. K., Brown, L. S., Needleman, R., and Lanyi, J. K. (1998) *Biochemistry 37*, 9889−9893.
39. Weidlich, O., Schalt, B., Friedman, N., Sheves, M., Lanyi, J. K., Brown, L. S., and Siebert, F. (1996) *Biochemistry 35*, 10807−10814.
40. Cao, Y., Brown, L. S., Needleman, R., and Lanyi, J. K. (1993) *Biochemistry 32*, 10239−10248.
41. Heberle, J., and Dencher, N. A. (1992) *Proc. Natl. Acad. Sci. U.S.A. 89*, 5996−6000.
42. Zimányi, L., Váró, G., Chang, M., Ni, B., Needleman, R., and Lanyi, J. K. (1992) *Biochemistry 31*, 8535−8543.
43. Brown, L. S., Gat, Y., Sheves, M., Yamazaki, Y., Maeda, A., Needleman, R., and Lanyi, J. K. (1994) *Biochemistry 33*, 12001−12011.
44. Smith, S. O., Pardoen, J. A., Mulder, P. P. J., Curry, B., Lugtenburg, J., and Mathies, R. (1983) *Biochemistry 22*, 6141−6148.
45. Sasaki, J., Lanyi, J. K., Needleman, R., Yoshizawa, T., and Maeda, A. (1994) *Biochemistry 33*, 3178−3184.
46. Luecke, H., Schobert, B., Richter, H. T., Cartailler, J. P., and Lanyi, J. K. (1999) *J. Mol. Biol. 291*, 899−911.
47. Yamazaki, Y., Hatanaka, M., Kandori, H., Sasaki, J., Karstens, W. F. J., Raap, J., Lugtenburg, J., Bizounok, M., Herzfeld, J., Needleman, R., Lanyi, J. K., and Maeda, A. (1995) *Biochemistry 34*, 7088−7093.
48. Alexiev, U., Marti, T., Heyn, M. P., Khorana, H. G., and Scherrer, P. (1994) *Biochemistry 33*, 298−306.
49. Kimura, Y., Vassylyev, D. G., Miyazawa, A., Kidera, A., Matsushima, M., Mitsuoka, K., Murata, K., Hirai, T., and Fujiyoshi, Y. (1997) *Nature 389*, 206−211.
50. Checover, S., Marantz, Y., Nachliel, E., Gutman, M., Pfeiffer, M., Tittor, J., Oesterhelt, D., and Dencher, N. A. (2001) *Biochemistry 40*, 4281−4292.
51. Brown, L. S., Needleman, R., and Lanyi, J. K. (1999) *Biochemistry 38*, 6855−6861.
52. Riesle, J., Oesterhelt, D., Dencher, N. A., and Heberle, J. (1996) *Biochemistry 35*, 6635−6643.
53. Checover, S., Nachliel, E., Dencher, N. A., and Gutman, M. (1997) *Biochemistry 36*, 13919−13928.
54. Zscherp, C., Schlesinger, R., Tittor, J., Oesterhelt, D., and Heberle, J. (1999) *Proc. Natl. Acad. Sci. U.S.A. 96*, 5498−5503.
55. Bressler, S., Friedman, N., Li, Q., Ottolenghi, M., Saha, C., and Sheves, M. (1999) *Biochemistry 38*, 2018−2025.
56. Balashov, S. P., Lu, M., Imasheva, E. S., Govindjee, R., Ebrey, T. G., Othersen, B., III, Chen, Y., Crouch, R. K., and Menick, D. R. (1999) *Biochemistry 38*, 2026−2039.
57. Li, Q., Bressler, S., Ovrutsky, D., Ottolenghi, M., Friedman, N., and Sheves, M. (2000) *Biophys J. 78*, 354−362.
58. Rath, P., Bovee-Geurts, P. H., DeGrip, W. J., and Rothschild, K. J. (1994) *Biophys. J. 66*, 2085−2091.

BI011027D